RILEM-*fib*-AFGC Int. Symposium on Ultra-High Performance Fibre-Reinforced Concrete,
UHPFRC 2013 – October 1-3, 2013, Marseille, France

ASSESSMENT OF COUPLED THERMO-MECHANICAL BEHAVIOUR OF ULTRA HIGH PERFORMANCE CONCRETE COLUMNS IN CASE OF FIRE

Matthias Siemon (1) and Dietmar Hosser (1)

(1) Institute of Building Materials (iBMB), Braunschweig Institute of Technology, Germany

Abstract

This paper presents the investigations on the coupled thermo-mechanical behavior of UHPFRC in case of fire. For the thermal properties like thermal conductivity and thermal diffusivity the transient plane source method (TPS) has been used, the specific heat and the mass loss were determined via differential scanning calorimeter and the thermo gravimetric analysis. The mechanical properties like the temperature-dependent stress-strain relations and the thermal expansion were derived using steady-state and transient tests as well as middle-scale experiments for the assessment of the spalling behavior. As a result, the temperature dependent strength and stress-strain relations were calculated by analogy to the data given in Eurocode 2 for normal strength concrete. To check the practicability of the data, real scale experiments assessing the characteristics of UHPFRC columns under combined mechanical and thermal load were carried out, providing detailed information on the displacement behavior.

Résumé

Ce document présente un travail de recherche sur le comportement couplé thermo-mécanique des BFUP en situation d'incendie. La méthode de la « source plane transitoire » a été utilisée afin de déterminer les propriétés thermiques comme la conductivité thermique et la diffusivité thermique. La chaleur spécifique et la perte de poids ont été déterminées par calorimétrie différentielle à balayage et analyse thermogravimétrique. Les propriétés mécaniques comme la relation contrainte-déformation et la dilatation thermique ont été déterminées en réalisant des essais statiques et transitoires. Des essais sur des corps d'épreuve d'échelle intermédiaire ont également été réalisés afin d'évaluer la propension à l'écaillage de ces bétons étudiés. Ensuite, les résistances et les courbes contrainte-déformation qui dépendent de la température ont été développées par analogie avec les données de l'Eurocode 2 pour les bétons de résistance normale. Pour vérifier la justesse des données, des essais à échelle réelle ont été réalisés sur des colonnes UHPC sous charge mécanique et thermique combinée afin d'obtenir des informations détaillées sur les déplacements.

1. INTRODUCTION

In this paper the behaviour of ultra high performance fibre reinforced concrete (UHPFRC) exposed to fire was assessed using two defined mixtures which were developed in the German

research program SPP 1182. The first one is a mortar named M3Q, the second one a concrete named B5Q. Compared to normal strength concrete, UHPC shows brittle failure behaviour which is unwanted for building components under compression load. This is due to the fact that no warning signs (e.g. large strains) are apparent. To provide ductile failure behaviour, steel fibres were added to the concrete mixture, having an effect on the softening of the material after reaching its ultimate strength. Additionally, PP-fibres are added to protect the UHPC members from explosive spalling when exposed to fire. The underlying protection mechanisms of the PP-fibres are not yet completely explained. A widely accepted explanation is the development of a pore system at temperatures of about 160 °C when the PP-fibres melt. This pore system is then capable of distributing the developing vapour pressure through the gained volume, and finally releasing it.

2. ASSESSED MIXTURES AND SPALLING BEHAVIOR

Details of the assessed UHPFRC mixtures, the mortar M3Q and the concrete B5Q can be found in table 1.

Table 1: Mixtures of UHPFRC M3Q (mortar) and B5Q (concrete) [1]

Material	**M3Q - Mass [kg/m^3]**	**B5Q - Mass [kg/m^3]**
Water	175	155
CEM I 52,5 R HS/NA	825	650
Microsilica	175	170
Liquifier	27.5	34.5
Quartz powder	200	456
Quartz sand 0.125/0.5	975	354
Basalt 2/5	0	298.5
Basalt 5/8	0	298.5
Steel fibres 0.19/9 mm	80 (1 Vol.-%)	80 - 201 (1 - 2.5 Vol.-%)
PP-fibres (polypropylene)	0 - 2.25 kg/m³	0 - 2.25 kg/m²
If the steel fibre contents differ from the ones described in this table they are explicitly given in the correspondent text passage.		

The effect of the PP-fibre content on the spalling behaviour was assessed during several small-scale and medium scale experiments. Beside the PP-fibre content, the load factor and additional protection barriers like mineral wool with different thickness, ablation coatings, intumescing painting and the content of steel fibres were varied. The loaded specimens vary in the amount of reinforcement. The results showed that unprotected specimens (without PP-fibres) of the mortar M3Q were completely destroyed when exposed to the standard ISO 834-1 fire curve. The concrete mixture B5Q was more resistant when exposed to fire. The results of the unprotected specimens are depicted in figure 1.

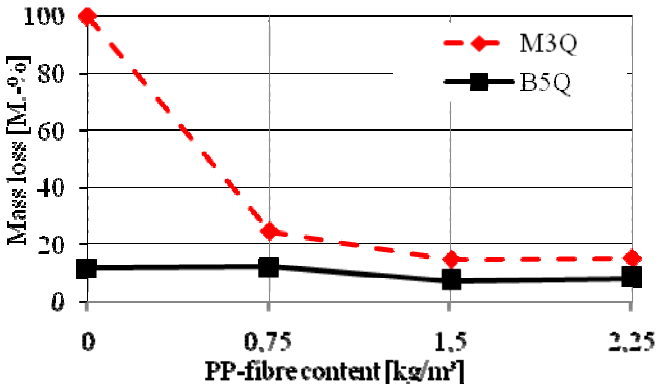

Figure 1: Mass loss of unprotected specimens depending on the PP-fibre content [1]

3. THERMAL MATERIAL PARAMETERS

For the proof of building components exposed to fire the temperature distribution in the cross-section is needed. The thermal analysis is carried out by solving the well-known transient thermal problem described by the Fourier equation depicted as eq. 1 for the two dimensional case:

$$\frac{\partial}{\partial x}\left(\lambda\frac{\partial T}{\partial x}\right)+\frac{\partial}{\partial y}\left(\lambda\frac{\partial T}{\partial y}\right)-\rho c_p\frac{\partial T}{\partial t}=-q \qquad (1)$$

In fire protection engineering, all parameters, the thermal conductivity λ, the density ρ and the specific heat capacity c_p are functions of the temperature. This yields to a nonlinear system of equations which is usually solved using a Newton-Raphson algorithm.

In the following sections, the experimental methods for the determination of these parameters and the results for the mixtures M3Q and B5Q are described. In all cases, the test specimens were stored for at least 100 days after 28 days of underwater storage. The moisture content for this case was determined between 2.5 to 3.2 M.-%

3.1 Temperature dependent heat conductivity

The temperature-dependent thermal conductivity λ was assessed utilizing the so-called TPS method (Transient Plane Source). In this transient experiment, a sensor is located and fixed between two concrete specimens. This sensor serves as a heating source as well as a temperature sensor. The results are then used to derive the conductivity λ. More information to this method can be viewed in DIN EN ISO 22007-2 [2].

The resulting temperature-dependent thermal conductivity λ is depicted for the concrete B5Q in figure 2.

The red dashed line on the bottom shows the values for normal strength concrete given by the Eurocode 2 part 1.2 [3]. The higher values for UHPFRC can be explained with the large fractions of fine powder components compared to normal concrete which yields a higher packing density of the cement matrix. The black line in figure 2 shows the temperature-dependent heat conductivity of UHPC used for the thermal analysis. The curve was derived from the experimental results of the B5Q with a PP-fibre content of 2.25 kg/m³.

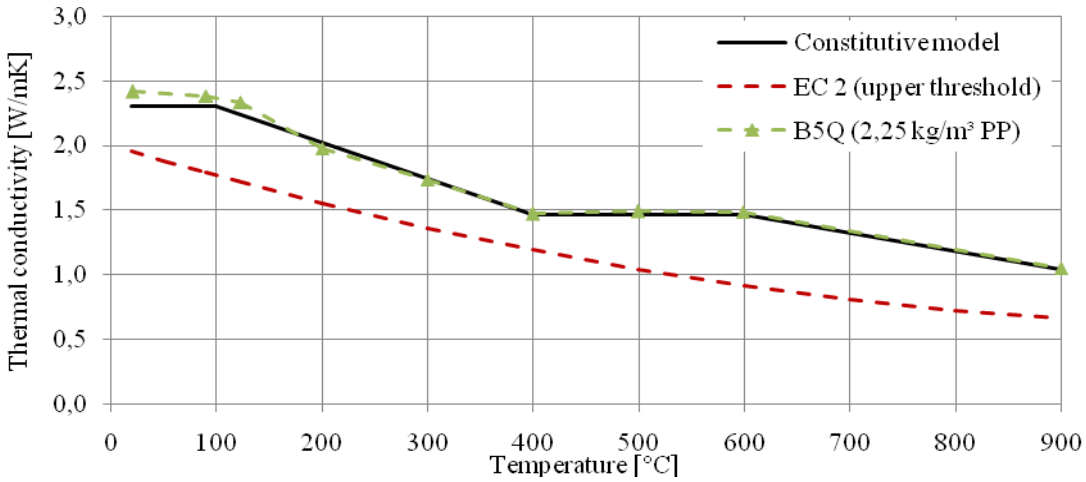

Figure 2: Thermal conductivity of the UHPC B5Q compared to the function of the Eurocode 2 and the derived function for the thermal calculation [1]

3.2 Temperature-dependent density ρ and specific heat capacity c_p

The parameters for the transient term of eq. 1 where determined using the Thermogravimetric Analysis (TGA) for the temperature-dependent density and the Differential Scanning Calorimetry (DSC) according to [4].

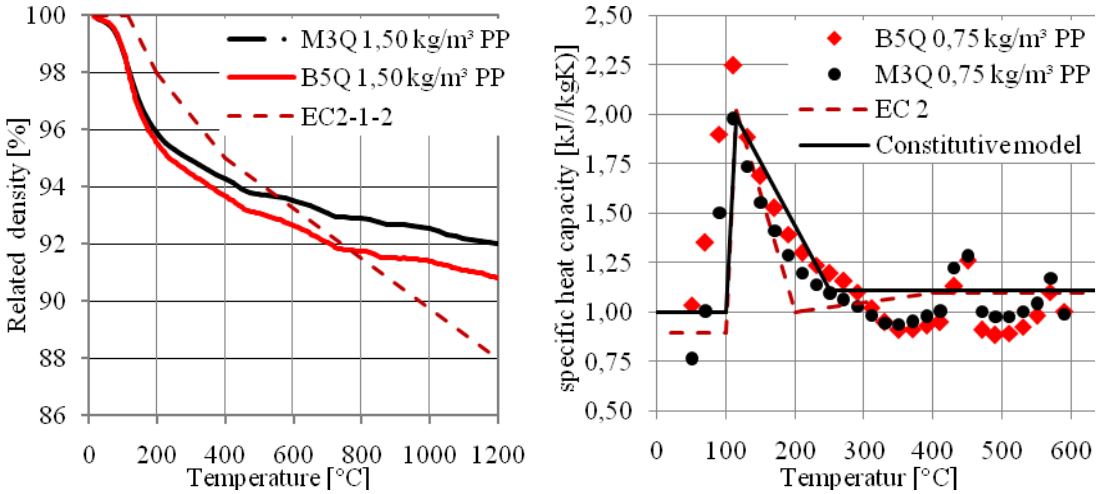

Figure 3: Temperature-dependent mass loss of the mixtures B5Q and M3Q (left) and specific heat capacity (right) [1]

Like done for the thermal conductivity, the resulting values for the mass loss as well as for the specific heat capacity are compared with the values for normal strength concrete [3]. Figure 3 (right) shows the characteristic peak of measured heat capacity starting at 100 °C when the free and physical bond water is evaporating. The two smaller peaks at 450 °C show the decomposition of Portlandite cement component and the transformation of quartzite aggregates, both endothermic reactions. The derived calculation model (black) and the model for normal strength concrete (dashed) [3] are also shown.

4. THERMO-MECHANICAL MATERIAL PARAMETERS

4.1 Temperature-dependent uniaxial stress-strain relationship

To describe the temperature-dependent mechanical behaviour of concrete, steady-state and transient tests on small-scale cylinder specimens were carried out. All relevant parameters like the heating rate, loading velocity and the general experimental setup were chosen in accordance to national and international guidelines and recommendations [5]. More detailed information on the execution of the experiments can be viewed in [1].

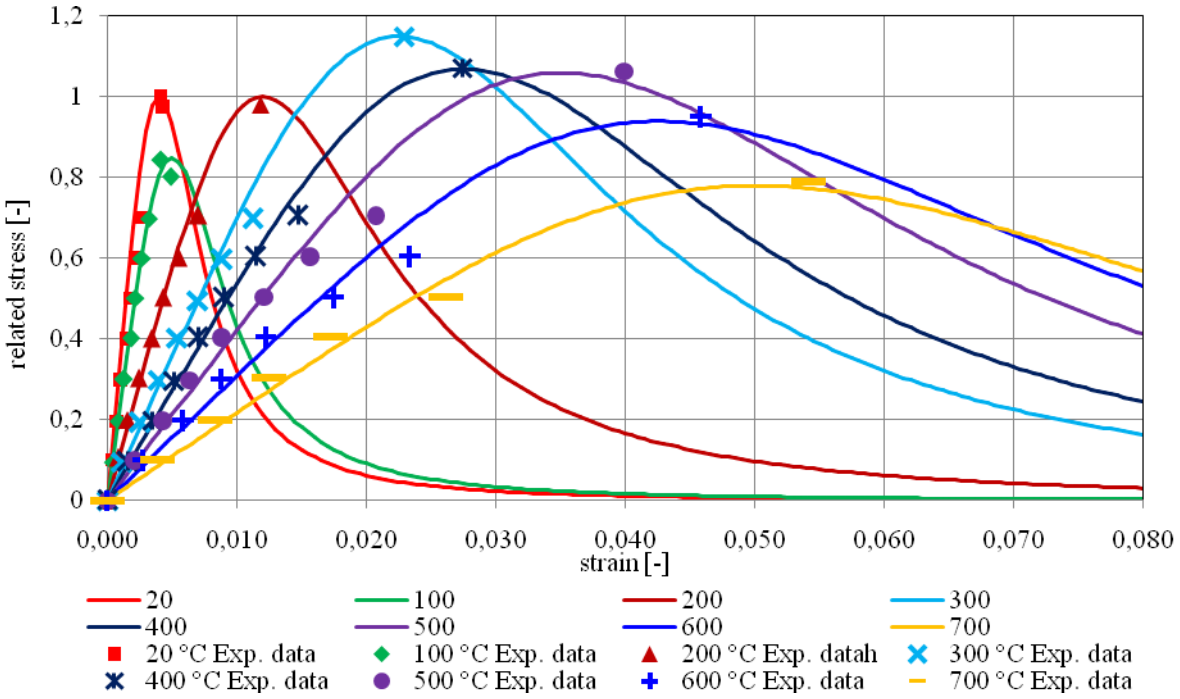

Figure 4: Temperature-dependent stress-strain relationships developed in SPP 1182 (including transient creep strains)

As a result of the steady-state tests, temperature-dependent compression strengths were determined. Combined with the results of the transient creep strain tests, a uniaxial stress-strain relation can be derived. Figure 4 shows this relation related to the compression strength at 20 °C. The experimental values are plotted as check marks (square, circle, triangle, etc). To describe a general uniaxial behaviour, the constitutional function described by Thorenfeldt [6], which was originally developed for UHPC and also used for the concrete model of the Eurocode 2 part 1.2 [3], was used. Eq. 2 shows the general formulation as described by Thorenfeldt [6]. The function used in the Eurocode 2 for normal strength concrete was derived from eq. 2 for nk=3.

$$\sigma(\theta) = f_c(\theta)\left(\frac{\varepsilon}{\varepsilon_{c1}(\theta)}\right)\left(\frac{n}{n-1+\left(\frac{\varepsilon}{\varepsilon_{c1}(\theta)}\right)^{nk}}\right) \tag{2}$$

As it can be viewed in figure 4, it fits the experimental results quite well. Unfortunately, due to the nature of the transient creep tests, no values for the softening branch where captured. Due to its classification as mortar, a further look on the mixture M3Q is resigned at this point. The large scale tests were also carried out on columns made of UHPFRC B5Q.

4.2 Biaxial constitutive model

The boundary conditions of the large scale columns tests with two-dimensional nonlinear heat transfer as well as geometrical and physical nonlinearities in the mechanical model made it necessary to utilize a solid element model for the validation of the material model. In this case, the FE-Software DIANA offers two different approaches, a so-called Total Strain Crack Model and several elasto-plastic models [7]. For this work, the first model showed severe convergence and bifurcation problems due to the softening behaviour when exposed to high temperature boundary conditions. Because of this, a multi failure surface isotropic plasticity model (combined Drucker-Prager / Rankine yield criteria) was used for two-dimensional problems and standard Drucker-Prager model for three-dimensional problems. The derivation of the constitutive model from the uniaxial data is presented in the next section. It was implemented as a user-supplied subroutine written in Fortran.

The Drucker-Prager yield function depending on the parameters α_g and β as well as from a hardening function $c(\kappa)$ is depicted in eq. 3. The formulation for the combined DP-Rankine multi-surface model can be viewed in [7].

$$F^{DP}(\sigma,\kappa)=\sqrt{\frac{1}{2}\sigma^{T}\begin{bmatrix}2&-1&-1&0&0&0\\-1&2&-1&0&0&0\\-1&-1&2&0&0&0\\0&0&0&6&0&0\\0&0&0&0&6&0\\0&0&0&0&0&6\end{bmatrix}\sigma}+\alpha_g\begin{Bmatrix}1\\1\\1\\0\\0\\0\end{Bmatrix}^{T}\sigma-\beta c(\kappa)\le 0 \tag{3}$$

As described in [7], the uniaxial experimental data can be translated into a cohesion-internal state function based on a cohesion hardening material. This engineering approach is based on the assumption that the friction and dilatancy angle is independent from the internal state variable as well as from the temperature. Although it is known from several biaxial experiments done at the iBMB that there is a temperature influence for normal strength concrete [8], this assumption will be used due to the lack of data for UHPC as a first attempt. Furthermore, the methodology is based on a strain-hardening assumption.

Eq. 5 describes the equivalent plastic strain derived from the total strain function. Together with the function of the cohesion (eq. 6) based on the function of eq. 2, a temperature-dependent cohesion-hardening relation defining the hardening and softening behavior of the yield surface is derived.

$$\kappa(\theta)=\left(\varepsilon(\theta)-\left(\frac{\sigma(\theta)}{E(\theta)}\right)\right)\cdot\sqrt{\left(1+\left(2\alpha_g{}^{2}\right)\right)/\left(1-\alpha_g\right)} \tag{4}$$

$$c(\kappa,\theta) = \sigma(\theta)\left(\frac{\kappa(\theta)}{\kappa_{c1}(\theta)}\right)\cdot\left(n/\left(n-1+\left(\frac{\kappa(\theta)}{\kappa_{c1}(\theta)}\right)^{nk}\right)\right)\cdot\left(\frac{1-\sin(\varphi)}{2\cos(\varphi)}\right) \quad (5)$$

A comparable approach for normal strength concrete is described by Schlegel in [9]. The parameters α_g and β (eq. 3) were fitted from biaxial tests at 20°C. The results are shown in figure 5. It shows the resulting yield surfaces for the maximum compression strength. The tensional behaviour was assumed to be elastic until σ_{ten} with a linear tension softening behaviour after that value. This approach was based on the findings on tensional behavior of UHPFRC in [10]. The maximum uniaxial compression strengths derived from figure 4 are marked with rectangles in figure 5.

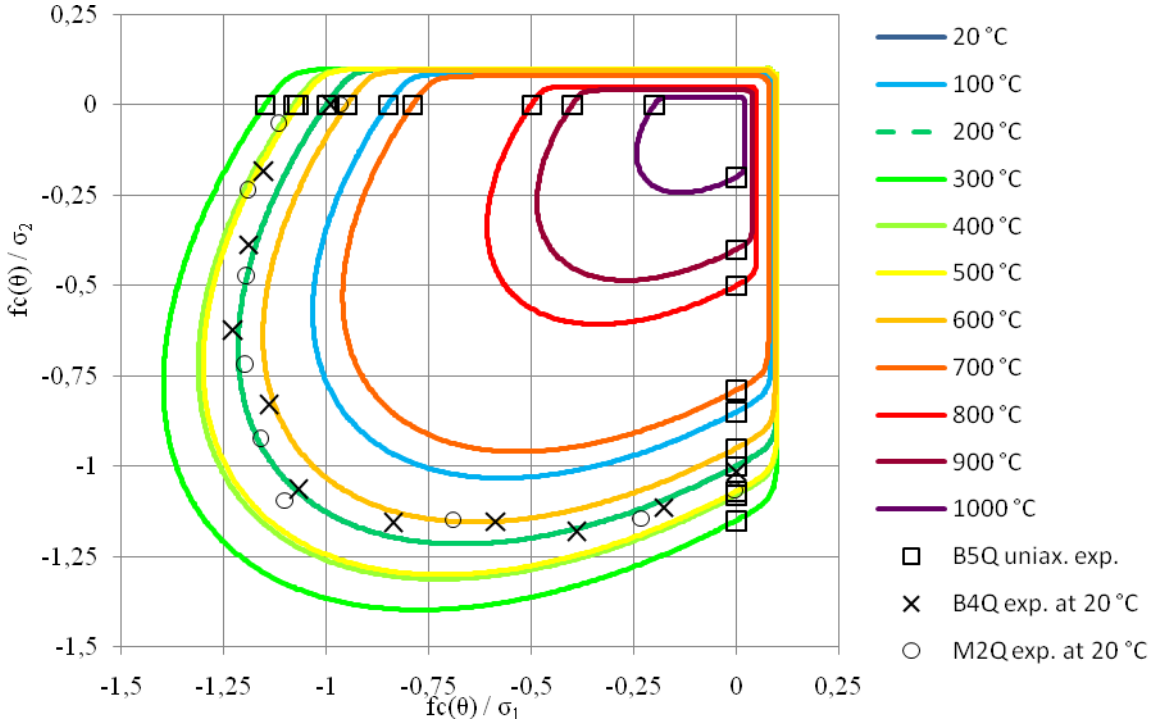

Figure 5: Temperature-dependent yield surfaces with biaxial experimental results at 20 °C and uniaxial experimental results [11]

The parameters α_g and β of the yield surface were calibrated with results from [11] derived from analysis of predecessor mixtures B4Q and M2Q. At this stage of the research project, different steel fibres were tested. For the depicted results in figure 5, the mixtures B4Q and M2Q use the same steel fibres as the successor mixtures B5Q and M3Q. The other components and mixture ratios were the same as for the mixtures B5Q and M3Q.

5. VALIDATION CALCULATIONS

5.1 Small scale transient tests for mixture B5Q

The dimensions of the assessed specimens where 80 mm in diameter and 240 mm in height and the specimens were loaded with 0 % up to 70 % of the cold compression strength.

Figure 6 shows the measured and calculated transient strains using the constitutive model developed in section 4. It can be seen that there is a little underestimation of the strains for small load ratios as well as for high ratios. Overall, the model was capable of calculating the transient strains recorded in the experiments quite well. The model was based on axi-symmetric two-dimensional quadrilateral elements.

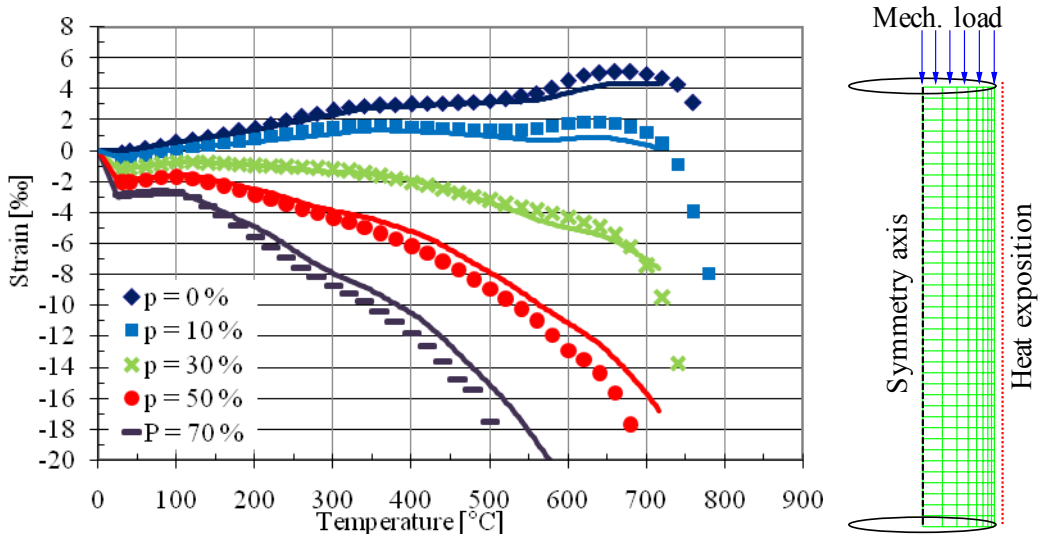

Figure 6: Experimental results and calculation (continuous lines) of transient creep strain tests (left), axisymmetric FE-model used (right)

5.2 Large scale columns exposed to fire (B5Q)

The columns had a height of 3.7 m with hinged supports at both ends, realized with steel plates. The cross-section with the dimension of 30 cm x 30 cm was reinforced with eight reinforcement bars of B 500 with a diameter of 20 mm. The binder reinforcement had a diameter of 10 mm with a margin of 20 cm between each binder. All four faces were exposed to temperatures according to the standard fire (ISO 834-1) using oil burners.

The mechanical load of 1800 kN was applied with a steel semicircular and had a small eccentricity of 7.5 mm and 15 mm to model on-site inaccuracy. The displacements were determined with a glass sensor at h/2 of the column over the whole duration of fire exposure until the failure of the column. Additionally, the temperatures were recorded at different heights and depth of the cross-section to validate the determined parameters as well as the coupled thermo-mechanical calculation model. The temperatures in the cross-section were determined with thermocouples mounted before the casting of the column. Due to the high packing density of UHPC, the thermocouples were completely covered by concrete and therefore not passed by water vapour during heating. This lead to a constant heat increase in the experimental data instead of the plateau at 100 °C, recorded in cases where the thermocouples are attached after casting, e.g. via bore holes, or generally for porous materials.

In a first step, the columns were mechanically loaded and the horizontal displacement was recorded. In a next step, the fire load was imposed, yielding to material degradation under fire exposure and as a result, to additional horizontal displacements and moment loading until failure of the column.

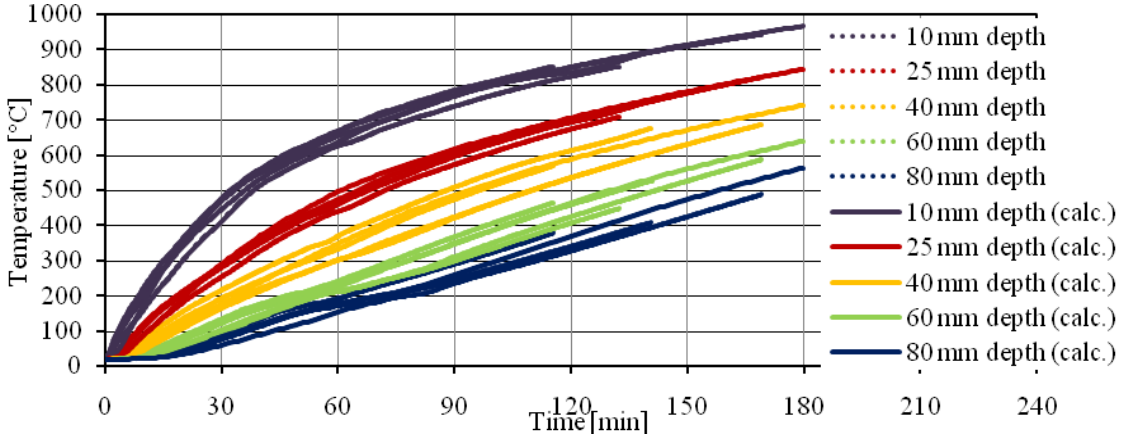

Figure 7: Cross-section temperatures in different depth and heights of the columns from experiments (dotted lines) and calculated values (continuous lines)

The thermal analysis was conducted with the experimental data described in section 3. Figure 7 shows a good accordance of the calculated temperatures with the ones measured in the experiments with the attached thermocouples. The consideration of water evaporation using a peak in the specific heat at 100 °C leads to a damping of the temperature development. Convective processes in capillary pore systems or heat sinks due to water evaporation were not considered in the applied mathematical model after eq. 1.

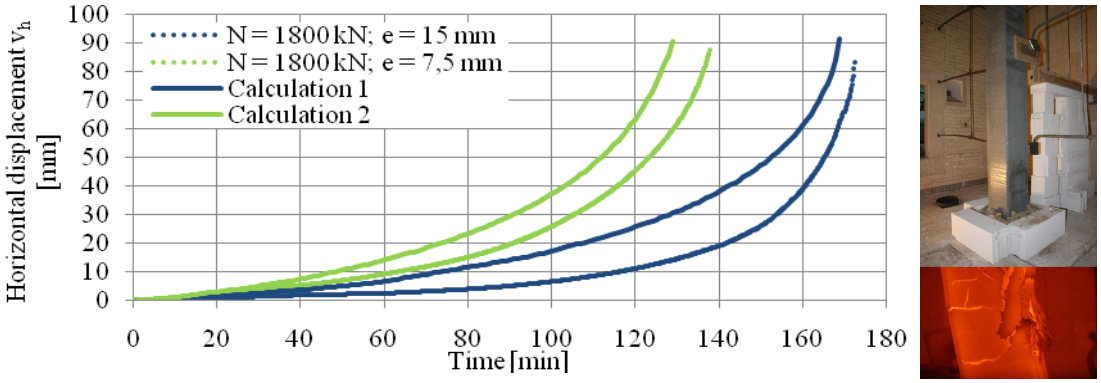

Figure 8: Horizontal displacements (continuous lines) of large scale colums compared to calculated values (left), pictures of the fire chamber (right)

The resulting horizontal displacements over the time are plotted in figure 8 as continuous lines. In general, the calculations seem to underestimate the stiffness of the columns recorded in the experiments. This yields to higher displacements as measured for each time step. The resulting failure times of 140 min (e = 15 mm) and 170 min (e = 7.5 mm) were underestimated by about 10 min.

6. CONCLUSIONS

As shown for the validation calculations, the calculation of the temperatures in the cross-section using the derived thermal material properties for UHPFRC is possible and the results fit the experimental data quite well. The derived thermo-mechanical constitutive model for an

adjacent structural analysis allows a general calculation of the material behaviour of UHPFRC, as it is shown in section 5.1 for small-scale tests. As shown in figure 8, calculations of large scale experiments show a slight underestimation of the component stiffness, resulting in larger displacements compared to the experimental results.

Future research work should focus on the assessment of a material model generally capable of describing the temperature-dependent behaviour of concrete utilizing state-of-the-art FE-methods based on extensive experimental research of the widened spectrum of concrete (HPC, UHPC).

ACKNOWLEDGEMENTS

The authors would like to acknowledge the German Research Foundation (DFG) for the support of the research project 'Theoretische und experimentelle Untersuchungen zur Ermittlung und Optimierung des Brandverhaltens von ultra-hochfestem Beton' (Theoretical and experimental studies for determining and optimizing the fire behaviour of ultra high performance concrete) in the priority program 1182.

REFERENCES

[1] Hosser, D., Kampmeier, B. and Hollmann, D., 'Behavior of Ultra High Performance Concrete (UHPC) in Case of Fire', in 'Ultra-High Performance Concrete and Nanotechnology in Construction: 3rd International Symposium on UHPC and Nanotechnology for High Performance Construction Materials', Proceedings of Hipermat 2012, Kassel, March 2012 (University Kassel) 573-582.

[2] DIN EN ISO 22007-2: Plastics – Determination of thermal conductivity and thermal diffusivity – Part 2: Transient plane heat source (hot disc) method.

[3] DIN EN 1992-1-2:2010-12 – Eurocode 2: Design of concrete structures – Part 1-2: General rules – Structural fire design; German version EN 1992-1-2:2004 + AC:2008

[4] DIN 51007:1994-06 – Thermische Analyse (engl.: thermal analysis) (TA); Differenzthermoanalyse (engl.: differential thermal analysis) (DTA); Grundlagen.

[5] Rilem TC 129 MHT: Test Methods for mechanical properties of concrete at high temperatures

[6] Thorenfeld, E., Tomaszewicz, A., Jensen, J. J., 'Mechanical properties of high-strength concrete and applications in design', in 'Proc. Symp. Utilization of High-Strength Concrete', Stavanger, Norway, 1987 (Trondheim)

[7] de Witte, F. C., Kikstram W. P., 'DIANA- Finite Element Analysis – Users manual release 9 – Material library, First edition, TNO DIANA, Delft, The Netherlands, 2005

[8] Thienel, K.-C., 'Festigkeit und Verformung von Beton bei hoher Temperatur und biaxialer Beanspruchung – Versuche und Modellbildung, DAfStb Heft 437, Berlin, 1994

[9] Schlegel, R., 'Nichtlineare Berechnung von Beton und Stahlbetonstrukturen nach DIN 1045-1 mit ANSYS (engl.: Nonlinear calculations of concrete and reinforced concrete after DIN 1045-1 using ANSYS)', '23rd CADFEM Users' Meeting 2005 – International Congress on FEM Technology', Bonn, November 2005, (International Congress Center Bundeshaus Bonn)

[10] Scheydt, J. C., Millon, O., Müller, H. S., Thoma, K., 'Entwicklung eines brandbeständigen ultrahochfesten Betons für hochdynamische Beanspruchung ', Beton- und Stahlbetonbau 107 (2012), Heft 5, Berlin, 2012

[11] Curbach, M., Speck, K., 'Versuchstechnische Ermittlung und mathematische Beschreibung der mehraxialen Festigkeit von ultra-hochfestem Beton (UHPC) – zweiaxiale Druckfestigkeit', Arbeitsbericht an die Deutsche Forschungsgemeinschaft (DFG) zum Forschungsvorhaben CU 37/6-1 im Rahmen des Schwerpunktprogramms 1182, Dresden, April 2007